LANGMUIR

Article

pubs.acs.org/Langmuir

Suppression of Photoanodic Surface Oxidation of n-Type 6H-SiC Electrodes in Aqueous Electrolytes

Matthias Sachsenhauser,[†] Karl Walczak,[‡,§] Paul A. Hampel,[†] Martin Stutzmann,[†] Ian D. Sharp,[‡,§] and Jose A. Garrido*[,∥,#]

[†]Walter Schottky Institut and Physik-Department, Technische Universität München, Am Coulombwall 4, 85748 Garching, Germany

[‡]Joint Center for Artificial Photosynthesis, Lawrence Berkeley National Laboratory, Berkeley, California 94720, United States

[§]Chemical Sciences Division, Lawrence Berkeley National Laboratory, Berkeley, California 94720, United States

[∥]Catalan Institute of Nanoscience and Nanotechnology (ICN2), CSIC and The Barcelona Institute of Science and Technology, Campus UAB, Bellaterra, 08193 Barcelona, Spain

[#]ICREA, Institució Catalana de Recerca i Estudis Avançats , 08070 Barcelona, Spain

Supporting Information

ABSTRACT: The photoelectrochemical characterization of silicon carbide (SiC) electrodes is important for enabling a wide range of potential applications for this semiconductor. However, photocorrosion of the SiC surface remains a key challenge, because this process considerably hinders the deployment of this material into functional devices. In this report, we use cyclic voltammetry to investigate the stability of n-type 6H-SiC photoelectrodes in buffered aqueous electrolytes. For measurements in pure Tris buffer, photogenerated holes accumulate at the interface under anodic polarization, resulting in the formation of a porous surface oxide layer. Two possibilities are presented to significantly enhance the stability of the SiC photoelectrodes. In the first approach, redox molecules are added to the buffer solution to kinetically facilitate hole transfer to these molecules, and in the second approach, water oxidation in the electrolyte is induced by depositing a cobalt phosphate catalyst onto the semiconductor surface. Both methods are found to effectively suppress photocorrosion of the SiC electrodes, as confirmed by atomic force microscopy and X-ray photoelectron spectroscopy measurements. The presented study provides straightforward routes to stabilize n-type SiC photoelectrodes in aqueous electrolytes, which is essential for a possible utilization of this material in the fields of photocatalysis and multimodal biosensing.

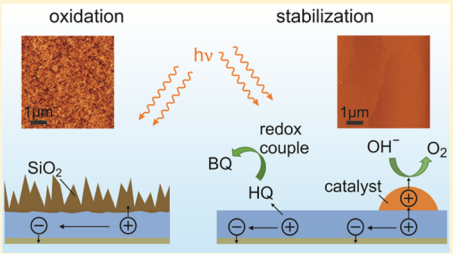

1. INTRODUCTION

Due to its outstanding mechanical stability and electronic properties, the wide bandgap semiconductor silicon carbide (SiC) has emerged as a promising material for applications in extreme conditions.[1] On the one hand, considerable effort is dedicated to the development of high-power and high-temperature electronics operating beyond the limitations of conventional silicon-based devices.[2−5] On the other hand, SiC also features an excellent chemical stability and biocompatibility, paving the way for implementations in the fields of photocatalysis and biosensing.[6−12] In this context, it has been demonstrated that SiC surfaces can be readily hydroxylated by etching in hydrofluoric acid,[13,14] which has been successfully used as a basis for covalent attachment of self-assembled monolayers to form functional organic/inorganic interfaces.[15−19] However, although organic molecules immobilized on SiC electrodes have proven to be stable under ultraviolet (UV) illumination in ambient conditions,[20] their utilization as passivation layers in photocatalytic or electro-optical biosensing applications also requires the long-term stability of the underlying SiC substrate material in active photoelectrochemical environments. In the literature, the photoelectrochemical properties of the most commonly used SiC polytypes have been investigated,[9,21−24] and it has been found that n-type electrodes severely corrode under photoanodic conditions,[9] even though the band edge positions at the surface are expected to be suitable to facilitate water oxidation in the electrolyte.[25] Considering the chemical inertness of SiC in acidic and alkaline environments, this corrosion process provides a powerful opportunity to create microstructures via photoelectrochemical etching,[26−29] which is highly relevant for the production of electronic or microelectromechanical devices. However, to advance the implementation of SiC photoelectrodes in photocatalytic or illuminated biosensing applications, suitable methods of suppressing photocorrosion in aqueous electrolytes have to be explored.

In this work, we investigate the stability of n-type 6H-SiC photoelectrodes in aqueous electrolytes. For this purpose, we employ cyclic voltammetry (CV) to study charge transfer processes across the SiC/electrolyte interface and focus on the

Received: November 30, 2015
Revised: January 18, 2016
Published: January 21, 2016

DOI: 10.1021/acs.langmuir.5b04376
Langmuir 2016, 32, 1637−1644

impact of photogenerated minority carriers on the photocorrosion of the SiC electrodes under above-bandgap illumination. In this context, the charge transfer characteristics across the SiC/electrolyte interface are analyzed in pure Tris buffer and in Tris buffer containing suitable redox couples (ferricyanide/ferrocyanide and benzoquinone (BQ)/hydroquinone (HQ)). In a further experiment, the SiC electrodes are modified with a cobalt phosphate (Co−Pi) catalyst, and its influence on the oxygen evolution reaction in the electrolyte is examined. As shown in Scheme 1, the energetic alignment of

Scheme 1. Energy Band Diagram of an n-Type 6H-SiC Electrode in Contact with an Aqueous Electrolyte (pH 7.3), Showing the SiC Band Edge Positions at a Bias Potential of U_{bias} = 0 V versus SHE and the H^+/H_2 and OH^-/O_2 Redox Potentials[a]

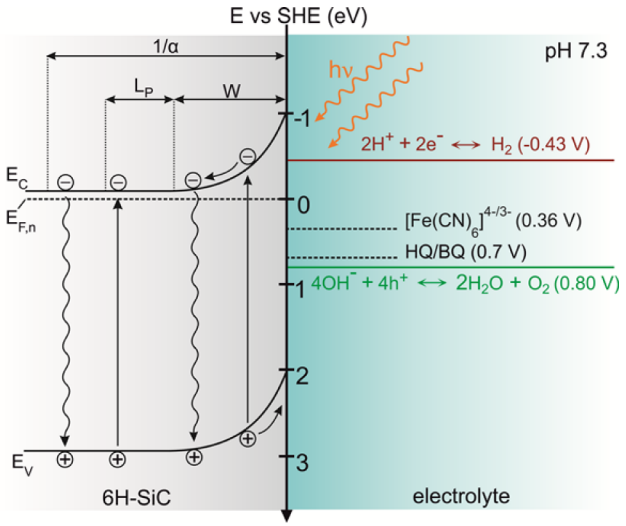

[a]The standard redox potentials of $[Fe(CN)_6]^{4-/3-}$ and BQ/HQ are also illustrated. Above-bandgap illumination results in the formation of electron−hole pairs within the absorption depth, $1/\alpha$. However, only those holes that are generated within the depletion layer width, W, and the minority carrier diffusion length, L_p, of the surface can facilitate oxidation reactions in the electrolyte. Charge transfer across the interface can occur either directly at the SiC band edges or be mediated by surface states located in the bandgap (not shown).

the band edge positions of n-type 6H-SiC with the relevant redox potentials in the electrolyte indicates that reduction processes rely on transfer of conduction band electrons, while the corresponding oxidation reactions require photogenerated holes from the valence band. In addition to the photoelectrochemical characterization, the surface stability with respect to photocorrosion is further evaluated using atomic force microscopy and X-ray photoelectron spectroscopy. Our results reveal that introducing suitable redox systems or depositing a Co−Pi catalyst are two straightforward routes to effectively suppress photo-oxidation of the SiC electrodes, thereby defining conditions under which the material can be stabilized and paving the way for their implementation in functional photoelectrochemical devices.

2. EXPERIMENTAL SECTION

2.1. Materials. Single-crystalline, (0001)-oriented n-type 6H-SiC wafers (nominal doping concentration $n \sim 1-2 \times 10^{18}$ cm^{-3}) were purchased from SiCrystal (Nürnberg, Germany) and chemomechanically polished to a root-mean-square (rms) surface roughness of 0.2 nm (NovaSiC, Le Bourget du Lac, France). Ohmic back contacts were prepared by annealing thermally evaporated NiCr/Au layers (50 nm each) at 1100 °C in vacuum (base pressure $p \sim 1 \times 10^{-8}$ mbar) for 3 min. Prior to (photo)electrochemical characterization, the substrates were cleaned by thorough sonication in acetone and isopropanol, followed by two cycles of oxygen plasma treatment (air-generated, 18 W, Harrick Plasma, Ithaca, NY) and etching in dilute hydrofluoric acid (5% in H_2O) for 5 min each. This treatment is known to yield clean, hydroxyl-terminated (0001) SiC surfaces.[13]

All chemicals and reagents were purchased from Sigma-Aldrich and used without further purification. Buffer solutions (50 mM Tris and 100 mM NaCl at pH 7.3) were prepared from Milli-Q water (ρ > 18 MΩ cm) and thoroughly degassed by nitrogen purging prior to use. Dependent upon the experiment, 1 mM potassium ferrocyanide (referred to as $[Fe(CN)_6]^{4-}$) or 1 mM HQ was added to the electrolyte. Because any UV absorbance of the buffer solutions can significantly influence the photoelectrochemical characteristics of the SiC electrodes, transmission spectra were recorded and are presented in Figure S1 of the Supporting Information.

2.2. Photoelectrochemical Characterization. A conventional three-electrode setup with a Ag/AgCl reference electrode (RE-5B from Bioanalytical Systems, Inc., West Lafayette, IN, 3 M NaCl, 0.196 V versus standard hydrogen electrode (SHE)) and a high-surface-area platinum wire counter electrode were used for photoelectrochemical characterization. Working electrodes were prepared by mounting the back-contacted 6H-SiC samples to a copper tape on a standard glass slide using conductive silver paste and then sealing the electrical connections from the electrolyte with a chemically resistant lacquer (Miccrostop lacquer, Tolber Chemical Division, Hope, AR). All CV experiments were conducted in a UV-transparent quartz beaker using a Bio-Logic SP-200 potentiostat (Bio-Logic SAS, France), and the obtained current values were normalized to the active sample area. Illumination with above-bandgap light was achieved using a spectroline ENF-260C lamp (Spectronics Corporation, Westbury, NY), providing selectable 254 and 365 nm emission with light intensities of 390 and 350 $\mu W/cm^2$, respectively. Unless stated otherwise, all potentials in this report are given relative to the Ag/AgCl reference electrode.

2.3. Co−Pi Catalyst Photodeposition. A Co−Pi water oxidation catalyst was photodeposited similarly to the methods described in the literature.[30−32] Briefly, clean SiC electrodes were electrically connected to a platinum counter electrode in a two-electrode configuration. Both electrodes were immersed in a 100 mM potassium phosphate solution (pH 7) containing 0.5 mM cobalt chloride. Photodeposition was then achieved by irradiating the samples for 10 min with a UV lamp (254 nm and 390 $\mu W/cm^2$). The functionalized SiC electrodes were rinsed in Milli-Q water and immediately used for photoelectrochemical characterization.

2.4. Atomic Force Microscopy (AFM). AFM was performed using a Veeco MultiMode system with a Nanoscope V controller in tapping mode. Topology data (5 × 5 μm^2) were acquired with silicon cantilevers at a typical scan frequency of 1 Hz, and the WSxM software suite (Nanotec Electronica S.L., Spain) was used for data processing and roughness analysis.[33]

2.5. X-ray Photoelectron Spectroscopy (XPS). XPS measurements were performed in a custom-built UHV system (base pressure p < 5 × 10^{-9} mbar) using a SPECS XR-50 Mg Kα X-ray source ($E_{K\alpha}$ = 1253.6 eV) and a SPECS Phoibos 100 hemispherical analyzer equipped with an MCD-5 detector. High-resolution spectra were recorded at a constant pass energy of 25 eV and a takeoff angle of 0° relative to the surface normal. After Shirley background subtraction, the individual core level spectra were normalized to the total spectrum intensity, taking into account the atomic sensitivity factors for each element.

3. RESULTS AND DISCUSSION

To study charge transfer processes of n-type 6H-SiC electrodes in aqueous electrolytes, cyclic voltammograms were recorded in pure Tris buffer without additional redox couples in the dark and under 365 and 254 nm illumination (see Figure 1). At large

DOI: 10.1021/acs.langmuir.5b04376
Langmuir 2016, 32, 1637−1644

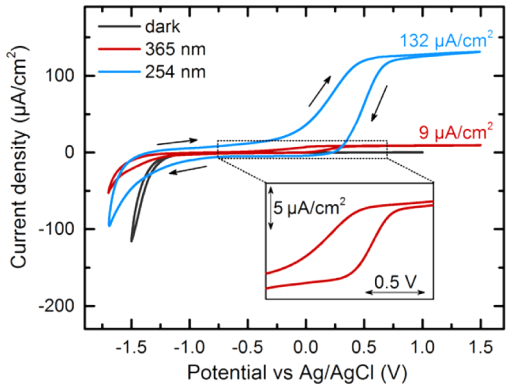

Figure 1. Cyclic voltammograms of an n-type 6H-SiC electrode in the dark (black line) and under 365 nm (red line) and 254 nm (blue line) illumination, revealing anodic photocurrents of 9 and 132 μA/cm^2 at 1.5 V versus Ag/AgCl, respectively. The measurements were recorded in Tris buffer (pH 7.3) at a scan rate of 250 mV/s. The inset shows a zoom to the potential region in which the anodic photocurrent onsets under 365 nm illumination.

cathodic bias potentials, electrons are transferred from the SiC conduction band to the electrolyte, resulting in an exponentially increasing current due to the evolution of hydrogen. This process occurs with and without illumination, because it is exclusively governed by majority carriers in n-type SiC. Conversely, an anodic current is only observed when above-bandgap illumination is present. Since it originates from photogenerated holes, driven to the interface by the electric field associated with an upward surface band bending (see Scheme 1), the anodic photocurrent would ideally onset at the flatband potential, U_{fb}, of the SiC electrode. Using impedance spectroscopy, U_{fb} was determined to be at −1.1 V versus Ag/AgCl in the dark (see Figure S2 of the Supporting Information). This indicates that a considerable overpotential is required to facilitate an anodic photocurrent under 365 and 254 nm illumination. Such a delayed onset is commonly observed for semiconductor electrodes and is typically explained by recombination of photogenerated electron−hole pairs in the space charge region or at electrically active surface states within the semiconductor bandgap.[34] In particular, surface states can trap photogenerated holes, and the accumulation of positive charges at the SiC/electrolyte interface results in an unpinning of the SiC band edges, thereby causing high surface recombination rates.[35] This effect can become even more pronounced in the case of slow charge carrier transfer kinetics, as is often observed for wide bandgap semiconductors and kinetically sluggish redox reactions.[36,37] When the potential is swept to more anodic values, the magnitude of the upward surface band bending increases and a continuously rising anodic current is observed. For potentials more positive than 0.2 and 0.6 V versus Ag/AgCl under 365 and 254 nm illumination, respectively, the photocurrent eventually flattens, because recombination losses in the space charge region and at the surface become negligible. It has to be pointed out, though, that the photocurrent does not saturate to a completely constant value but still moderately increases with potential for both photon energies. This behavior is in accordance with the Gärtner model,[38] which predicts an increase of the anodic photocurrent with increasing surface band bending as long as the absorption depth, $1/\alpha$, is larger than the sum of the space-charge layer width, W, and the minority carrier diffusion length, L_P (see Scheme 1). The 6H-SiC electrodes investigated in this work feature absorption depths of 12.5 μm and 250 nm for 365 and 254 nm illumination, respectively.[39] In contrast, the minority carrier diffusion length is expected to be smaller than 150 nm,[22] and the width of the space charge layer does not exceed 37 nm in the investigated potential range. Thus, for both illumination wavelengths, the concentration of holes, which are generated within $L_P + W$ and, therefore, contribute to the photocurrent, increases upon sweeping to more anodic potentials due to the potential dependence of W

$$W = \sqrt{\frac{2\varepsilon_{SC}\varepsilon_0}{eN_D}\left|(U_{bias} - U_{fb}) - \frac{k_B T}{e}\right|} \quad (1)$$

where ε_{SC} is the dielectric constant of SiC, ε_0 is the vacuum permittivity, e is the elementary charge, N_D is the donor density of the SiC electrode, k_B is the Boltzmann constant, and T is the absolute temperature. Interestingly, significantly different photocurrent magnitudes are observed for 365 and 254 nm illumination (9 versus 132 μA/cm^2 at 1.5 V versus Ag/AgCl). Considering that the light intensity of both wavelengths is very similar (see Experimental Section), this effect must be mainly caused by the wavelength dependence of the absorption depth of 6H-SiC. As mentioned above, values of 12.5 μm and 250 nm are expected for 365 and 254 nm illumination, respectively. This means that, for 365 nm photons, a significantly higher fraction of the electron−hole pairs is generated outside of $L_P + W$, i.e., recombination losses in the semiconductor bulk are more pronounced in comparison to 254 nm illumination.

As shown in Scheme 1, the energetic position of the valence band edge should be suitable to drive the oxygen evolution reaction in the electrolyte under above-bandgap illumination, by either direct or surface state mediated hole transfer across the interface. In this case, however, a corresponding oxygen

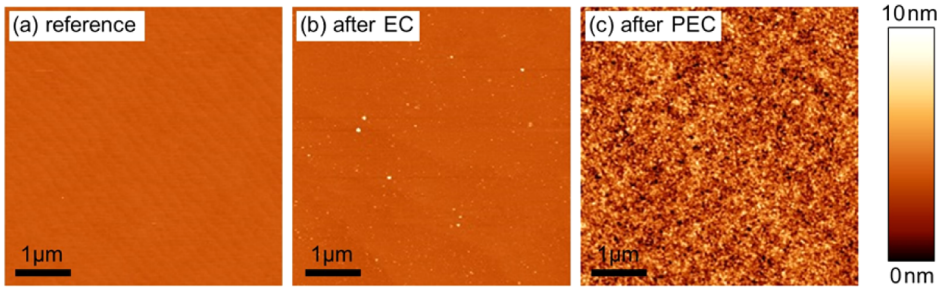

Figure 2. AFM images of 6H-SiC electrodes (a) after HF etching, (b) after electrochemical characterization in the dark, and (c) after photoelectrochemical characterization under above-bandgap illumination. The surface rms roughness values are 0.2, 0.3, and 1.6 nm, respectively. The z-scale is 10 nm for all images.

DOI: 10.1021/acs.langmuir.5b04376
Langmuir 2016, 32, 1637−1644

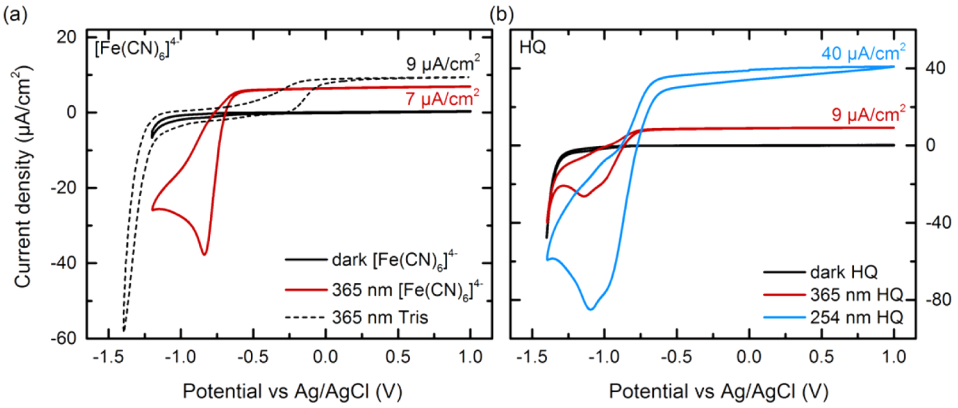

Figure 3. Cyclic voltammograms of 6H-SiC electrodes in Tris buffer containing (a) 1 mM $[Fe(CN)_6]^{4-}$, and (b) 1 mM HQ. The solid black lines show measurements recorded in the dark, and the red and blue lines depict the CV curves under 365 and 254 nm illumination, respectively. For comparison, a photoelectrochemical measurement in pure Tris buffer is also provided in panel a (black dashed line). All curves were recorded at a scan rate of 100 mV/s.

reduction reaction of the product would be expected upon cathodic sweeping of the potential, which is not observed in the cyclic voltammograms shown in Figure 1. Furthermore, a substantial hysteresis is visible between forward and reverse scans. In a similar work on n-type gallium nitride, such a hysteresis was ascribed to trapping of photogenerated holes in surface states, resulting in a surface modification of the GaN electrodes.[40] Hence, the anodic photocurrent observed in the present study is likely related to photocorrosion of the SiC samples instead of oxygen formation in the electrolyte. The corrosion process has already been investigated in the literature[9] and is expected to be governed by two parallel reactions, one a four-hole reaction and the other an eight-hole reaction, proceeding according to the following equations:

$$SiC + 4h^+ + 2H_2O \rightarrow SiO + CO + 4H^+ \quad (2)$$

$$SiC + 8h^+ + 4H_2O \rightarrow SiO_2 + CO_2 + 8H^+ \quad (3)$$

To provide further evidence for photoanodic oxidation of the SiC electrodes, the samples were ultrasonically cleaned in deionized water after the CV experiments and the surface morphology was examined with AFM (Figure 2). For comparison, a reference sample was also measured after HF etching and features a clean surface with an rms roughness value of 0.2 nm (Figure 2a).[41] After electrochemical characterization in the dark (Figure 2b), the surface structure remains unaltered, i.e., the cathodic current associated with hydrogen evolution in the electrolyte does not induce decomposition of the SiC electrodes. The slight increase of the rms roughness to 0.3 nm is ascribed to organic contaminants, which could not be removed from the sample surface during ultrasonication. Conversely, measurements under above-bandgap illumination result in the formation of a corrosion layer, in combination with a substantial increase of the rms roughness to 1.6 nm (Figure 2c). Since only a minor decrease of the magnitude of the anodic photocurrent is observed in CV measurements under continuous illumination (see Figure S3 of the Supporting Information), it can be concluded that the surface layer, which is formed in the photoanodic potential range, is very porous and barely hinders charge transfer.

While photocorrosion of n-type SiC electrodes can be very useful for the fabrication of electronic devices, it considerably hinders the deployment of this material into photocatalytic or illuminated biosensing applications. Therefore, suitable redox molecules were added to the electrolyte, and their influence on the interfacial charge transfer characteristics was investigated. Figure 3a shows cyclic voltammograms of a 6H-SiC electrode recorded in Tris buffer containing 1 mM $[Fe(CN)_6]^{4-}$, i.e., only the reduced component of the redox couple was initially present in the electrolyte. In the dark, oxidation of $[Fe(CN)_6]^{4-}$ to $[Fe(CN)_6]^{3-}$ cannot occur, because the concentration of holes in the valence band is negligible and electron injection into the conduction band is energetically inhibited (see Scheme 1). Accordingly, no reduction peak appears in reverse scan direction. Under 365 nm illumination, an anodic photocurrent is observed, with a value of 7 $\mu A/cm^2$ at U_{bias} = 1 V versus Ag/AgCl. The lower value in comparison to the measurements in pure Tris buffer (represented by the dashed line in Figure 3a) can be explained by the $[Fe(CN)_6]^{4-}$-containing electrolyte, which partly absorbs the incident UV light (see Figure S1 of the Supporting Information). In addition, a pronounced reduction peak evolves under cathodic polarization. Therefore, it must be concluded that the photogenerated holes are used to oxidize $[Fe(CN)_6]^{4-}$ molecules rather than accumulating at the surface and driving photocorrosion reactions. This finding is further confirmed by the observation of a significant cathodic shift of the photocurrent onset and the absence of a hysteresis between forward and reverse scans compared to the measurements in pure Tris buffer. The reduction peak maximum was found to depend on the anodic vertex potential and the scan rate (see Figure S4 of the Supporting Information); i.e., it is directly related to the concentration of $[Fe(CN)_6]^{3-}$ molecules that are generated in the anodic potential range. We note that illumination with 254 nm photons did not induce any photocurrent in this experiment, because the incident UV light was entirely absorbed in the electrolyte (see Figure S1 of the Supporting Information).

In a further experiment, ferrocyanide was therefore replaced by HQ molecules. Qualitatively similar CV curves were obtained in this case (see Figure 3b); in the dark, no contribution of HQ to the interfacial charge transfer characteristics is observable, but under above-bandgap illumination, BQ molecules are formed at anodic potentials and, thus, a corresponding reduction peak emerges in reverse scan direction. However, in contrast to the measurements presented in Figure 3a, the reduction peak is composed of two components, because two consecutive electron transfer

DOI: 10.1021/acs.langmuir.5b04376
Langmuir 2016, 32, 1637−1644

reactions are required to reduce BQ to HQ. Additionally, as a result of a lower electron transfer rate constant, the peak position is shifted to more cathodic potentials compared to the $[Fe(CN)_6]^{4-}$ reduction reaction. In the anodic potential range, photocurrents of 9 and 40 $\mu A/cm^2$ are observed at U_{bias} = 1 V versus Ag/AgCl for 365 and 254 nm photons, respectively. These values are consistent with the transmission curve of the HQ-containing electrolyte, as illustrated in Figure S1 of the Supporting Information. It has to be noted, though, that the absorbance of the electrolyte at 254 nm increases with an increasing BQ concentration, and thus, the magnitude of the anodic photocurrent decreases between forward and reverse scans of the CV experiment (see blue curve in Figure 3b). Nevertheless, as a result of the higher photocurrent value under 254 nm illumination (in comparison to 365 nm illumination), a larger number of BQ molecules is generated during the anodic sweep, resulting in higher cathodic currents in the subsequent BQ reduction reaction. The dependence of the reduction peak maximum on the BQ concentration was again confirmed by varying the anodic vertex potential and the scan rate for both illumination wavelengths and is shown in Figures S5 and S6 of the Supporting Information.

In the previous discussion, we have demonstrated that the accumulation of photogenerated holes at the SiC surface can be avoided by adding suitable redox systems to the electrolyte. For photoelectrolysis, however, water oxidation has to be facilitated in the anodic potential range. Therefore, the SiC surface was functionalized with a Co−Pi catalyst, which has been successfully used to promote oxygen evolution on other semiconductor electrodes,[42−44] and cyclic voltammograms were acquired in pure Tris buffer without any additional redox couple present in the electrolyte (see Figure 4). Under

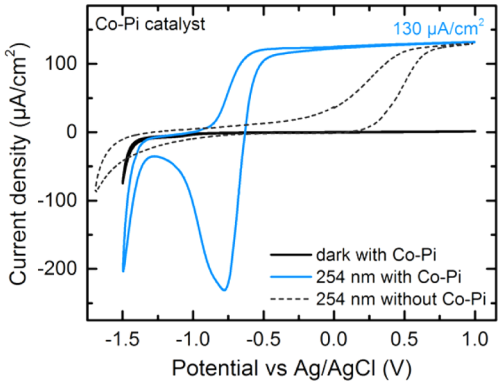

Figure 4. Cyclic voltammograms of a Co−Pi-functionalized 6H-SiC electrodes in pure Tris buffer. The black line shows a measurement in the dark, while the blue line depicts the respective curve under 254 nm illumination. For reference, a measurement without the catalyst attached to the SiC surface is also provided (dashed line). All curves were recorded at a scan rate of 100 mV/s.

254 nm illumination, a high photocurrent value of 130 $\mu A/cm^2$ is obtained at U_{bias} = 1 V versus Ag/AgCl. Importantly, a significant cathodic shift of 0.7 V versus Ag/AgCl in the photocurrent onset is observed relative to the bare SiC surface without a catalyst (similar to the measurements presented in Figure 3), which indicates that the Co−Pi catalyst facilitates transfer of photogenerated holes to the OH^-/O_2 redox couple in the electrolyte at anodic potentials. As a consequence, a pronounced cathodic peak is observed in the reverse scan direction, where the generated oxygen can be reduced by electrons from the SiC conduction band. To confirm that the observed reversible charge transfer behavior in fact originates from the OH^-/O_2 redox reaction and not from cobalt ions, which were adsorbed on the SiC surface during the Co−Pi deposition process, a CV curve of a catalyst-modified SiC electrode was also recorded without above-bandgap illumination (see black curve in Figure 4). In this case, only the reduction current associated with the hydrogen evolution reaction is observed, and no contribution of cobalt ions to the charge transfer characteristics appeared in the cyclic voltammogram.

The previous experiments provided several indications that redox molecules in the electrolyte or a Co−Pi catalyst deposited onto the surface considerably enhance the stability of n-type SiC photoelectrodes. However, unambiguous evidence on this stabilization effect cannot be obtained solely from CV experiments. The samples from Figures 3 and 4 were therefore cleaned by thorough ultrasonication after the CV measurements, and atomic force micrographs were recorded (see Figure 5). For comparison, the image from a sample that

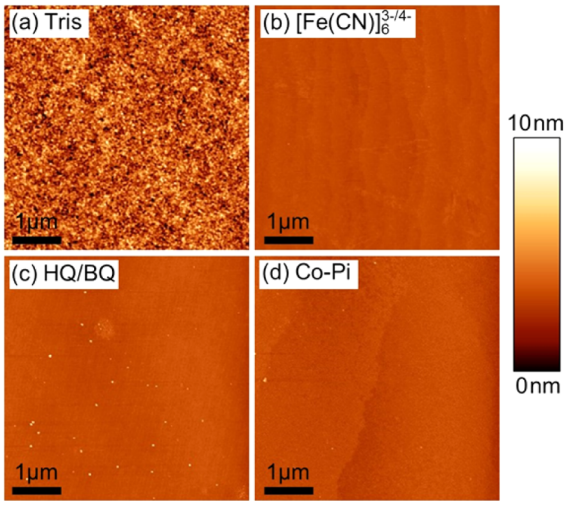

Figure 5. AFM images of 6H-SiC electrodes after photoelectrochemical characterization in (a) pure Tris buffer, (b) Tris buffer containing $[Fe(CN)_6]^{4-}$, (c) Tris buffer containing HQ, and (d) pure Tris buffer with a Co−Pi catalyst attached to the SiC surface. The surface rms roughness values are (a) 1.6 nm, (b) 0.2 nm, (c) 0.3 nm, and (d) 0.3 nm. The *z*-scale is 10 nm for all images.

was measured in pure Tris buffer and severely corroded in the photoelectrochemical testing conditions is again presented here (Figure 5a). In contrast to the topography for this corroded sample, measurements in the presence of redox molecules (panels b and c of Figure 5) or a catalyst (Figure 5d) reveal that there is not a significant increase in the surface rms roughness. Indeed, no significant modification of the surface morphology is observed.

To confirm the results from the AFM measurements and to obtain detailed information on the chemical composition of the SiC surfaces, the samples were further investigated with XPS. Figure 6 shows high-resolution Si2p (left panel) and O1s (right panel) core level spectra of the SiC electrodes (the corresponding survey scans and C1s spectra are provided in Figure S7 of the Supporting Information). For comparison, spectra that were obtained prior to photoelectrochemical characterization (after HF etching) are also depicted. In this

DOI: 10.1021/acs.langmuir.5b04376
Langmuir 2016, 32, 1637−1644

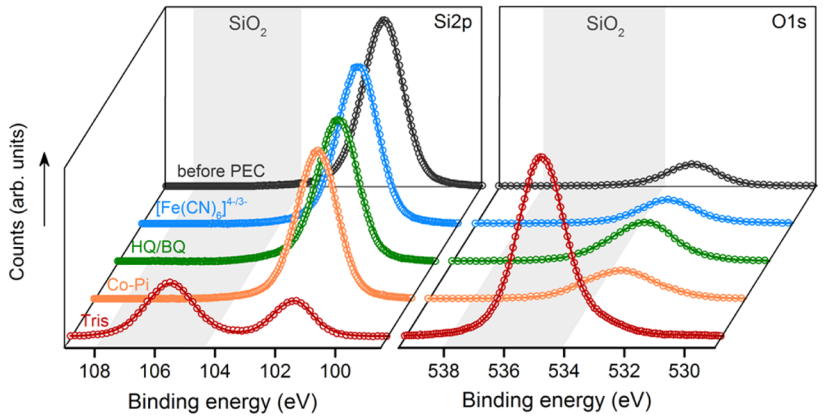

Figure 6. Si2p (left panel) and O1s (right panel) core level XPS spectra of 6H-SiC electrodes recorded after photoelectrochemical characterization in pure Tris buffer (red), in $[Fe(CN)_6]^{4-}$ buffer (blue), in HQ buffer (green), and with a Co−Pi catalyst attached to the surface (orange). For reference, measurements of an HF-etched sample are also depicted (black). Photoinduced surface oxidation is observed only in pure Tris buffer; all other samples are stable and do not exhibit photocorrosion during the photoelectrochemistry experiments.

case, the Si2p peak at 101.7 eV can be attributed to the SiC substrate, whereas the O1s signal at 533.1 eV originates from the hydroxyl surface termination after HF treatment[13] but also contains a contribution from water molecules that adsorb on the hydrophilic OH-terminated surface. Following photoelectrochemical characterization in pure Tris buffer, the chemical composition of the SiC surface changes significantly: the Si2p substrate signal at 101.7 eV is strongly attenuated, and a chemically shifted component at 105.7 eV emerges. At the same time, a substantial oxygen signal is observed at 535.0 eV. These changes confirm that a SiO_2 surface layer grows on the SiC electrodes during the photoelectrochemical corrosion process.[45] In contrast, no significant changes in the Si2p and O1s core level spectra are observed for all other samples operated under photoelectrochemical conditions, either in presence of a redox couple in solution or with a catalyst on the surface.[46] Hence, the AFM and XPS measurements confirm that the addition of suitable redox molecules to the electrolyte (e.g., $[Fe(CN)_6]^{4-}$ or HQ) or the deposition of an oxygen evolution reaction catalyst on the surface (e.g., Co−Pi) can suppress photocorrosion of 6H-SiC electrodes in aqueous electrolytes.

4. CONCLUSION

In this work, we have studied the photoelectrochemical stability of n-type 6H-SiC electrodes in aqueous electrolytes. For this purpose, we performed CV experiments and analyzed the charge transfer characteristics across the SiC/electrolyte interface. Under above-bandgap illumination, an anodic photocurrent, whose magnitude strongly depended on the applied potential and the incident photon energy, was observed. For measurements in pure Tris buffer, no indication of oxygen evolution was observed in the cyclic voltammograms, and consequently, the anodic current was exclusively ascribed to photocorrosion of the semiconductor surface. In an attempt to stabilize the SiC photoelectrodes, suitable redox molecules (ferrocyanide or HQ) were added to the electrolyte, which turned out to significantly influence the interfacial charge transfer characteristics; instead of accumulating at the surface and thereby corroding the electrode, the photogenerated holes were transferred to the reduced component of the redox couple, resulting in reversible photoanodic oxidation and cathodic reduction reactions. As an alternative to using redox species, a cobalt phosphate catalyst was deposited onto the SiC surface and was found to effectively suppress photoelectrochemical oxidation in favor of oxygen evolution in the electrolyte. To support the results from the CV measurements, AFM and XPS measurements were conducted, confirming that a SiO_2 surface layer was only formed in pure Tris buffer, while the redox molecules and the catalyst were suitable to avoid any modification of the SiC surface during photoelectrochemical characterization. In summary, our results provide straightforward opportunities to considerably enhance the stability of n-type SiC photoelectrodes in aqueous electrolytes, which is a basic prerequisite for implementing this material in photocatalytic and multimodal electro-optical biosensing applications.

■ ASSOCIATED CONTENT

Supporting Information

The Supporting Information is available free of charge on the ACS Publications website at DOI: 10.1021/acs.langmuir.5b04376.

Transmission spectra of buffer solutions (Figure S1), Mott−Schottky analysis of n-type 6H-SiC (Figure S2), additional cyclic voltammograms of 6H-SiC measured under above-bandgap illumination in pure Tris buffer (Figure S3) and in redox buffers (Figures S4−S6), and additional XPS data of 6H-SiC recorded after photoelectrochemical characterization (Figure S7) (PDF)

■ AUTHOR INFORMATION

Corresponding Author

*E-mail: joseantonio.garrido@icn.cat.

Notes

The authors declare no competing financial interest.

■ ACKNOWLEDGMENTS

Matthias Sachsenhauser acknowledges support of the IGSSE and of the Technische Universität München - Institute for Advanced Study, funded by the German Excellence Initiative. Ian D. Sharp was supported by the Joint Center for Artificial Photosynthesis, a DOE Energy Innovation Hub, supported through the Office of Science of the U.S. Department of Energy under Award Number DE-SC0004993.

DOI: 10.1021/acs.langmuir.5b04376
Langmuir 2016, 32, 1637−1644

REFERENCES

(1) Harris, G. L. *Properties of Silicon Carbide*; INSPEC, Institution of Electrical Engineers (IEE): London, U.K., 1995.

(2) Bhatnagar, M.; Baliga, B. J. Comparison of 6H-SiC, 3C-SiC, and Si for power devices. *IEEE Trans. Electron Devices* **1993**, *40*, 645−655.

(3) Weitzel, C. E.; Palmour, J. W.; Carter, C. H.; Moore, K.; Nordquist, K. K.; Allen, S.; Thero, C.; Bhatnagar, M. Silicon carbide high-power devices. *IEEE Trans. Electron Devices* **1996**, *43*, 1732−1741.

(4) Casady, J. B.; Johnson, R. W. Status of silicon carbide (SiC) as a wide-bandgap semiconductor for high-temperature applications: A review. *Solid-State Electron.* **1996**, *39*, 1409−1422.

(5) Neudeck, P. G.; Garverick, S. L.; Spry, D. J.; Chen, L.-Y.; Beheim, G. M.; Krasowski, M. J.; Mehregany, M. Extreme temperature 6H-SiC JFET integrated circuit technology. *Phys. Status Solidi A* **2009**, *206*, 2329−2345.

(6) Yang, N.; Zhuang, H.; Hoffmann, R.; Smirnov, W.; Hees, J.; Jiang, X.; Nebel, C. E. Nanocrystalline 3C-SiC Electrode for Biosensing Applications. *Anal. Chem.* **2011**, *83*, 5827−5830.

(7) Yakimova, R.; Petoral, R. M.; Yazdi, G. R.; Vahlberg, C.; Lloyd Spetz, A.; Uvdal, K. Surface functionalization and biomedical applications based on SiC. *J. Phys. D: Appl. Phys.* **2007**, *40*, 6435−6442.

(8) Inoue, T.; Fujishima, A.; Konishi, S.; Honda, K. Photoelectrocatalytic reduction of carbon dioxide in aqueous suspensions of semiconductor powders. *Nature* **1979**, *277*, 637−638.

(9) Lauermann, I.; Memming, R.; Meissner, D. Electrochemical Properties of Silicon Carbide. *J. Electrochem. Soc.* **1997**, *144*, 73−80.

(10) Akikusa, J. Photoelectrolysis of water to hydrogen in p-SiC/Pt and p-SiC/ n-TiO2 cells. *Int. J. Hydrogen Energy* **2002**, *27*, 863−870.

(11) van Dorp, D. H.; Hijnen, N.; Di Vece, M.; Kelly, J. J. SiC: A Photocathode for Water Splitting and Hydrogen Storage. *Angew. Chem., Int. Ed.* **2009**, *48*, 6085−6088.

(12) Guo, J.; Xiong, S.; Wu, X.; Shen, J.; Chu, P. K. *In situ* probing of intracellular pH by fluorescence from inorganic nanoparticles. *Biomaterials* **2013**, *34*, 9183−9189.

(13) Starke, U.; Bram, C.; Steiner, P.-R.; Hartner, W.; Hammer, L.; Heinz, K.; Müller, K. The (0001)-surface of 6H-SiC: morphology, composition and structure. *Appl. Surf. Sci.* **1995**, *89*, 175−185.

(14) Dhar, S.; Seitz, O.; Halls, M. D.; Choi, S.; Chabal, Y. L.; Feldman, L. C. Chemical Properties of Oxidized Silicon Carbide Surfaces upon Etching in Hydrofluoric Acid. *J. Am. Chem. Soc.* **2009**, *131*, 16808−16813.

(15) Rosso, M.; Arafat, A.; Schroen, K.; Giesbers, M.; Roper, C. S.; Maboudian, R.; Zuilhof, H. Covalent attachment of organic monolayers to silicon carbide surfaces. *Langmuir* **2008**, *24*, 4007−4012.

(16) Schoell, S. J.; Hoeb, M.; Sharp, I. D.; Steins, W.; Eickhoff, M.; Stutzmann, M.; Brandt, M. S. Functionalization of 6H-SiC surfaces with organosilanes. *Appl. Phys. Lett.* **2008**, *92*, 153301.

(17) Rosso, M.; Giesbers, M.; Arafat, A.; Schroen, K.; Zuilhof, H. Covalently Attached Organic Monolayers on SiC and SixN4 Surfaces: Formation Using UV Light at Room Temperature. *Langmuir* **2009**, *25*, 2172−2180.

(18) Auernhammer, M.; Schoell, S. J.; Sachsenhauser, M.; Liao, K.-C.; Schwartz, J.; Sharp, I. D.; Cattani-Scholz, A. Surface functionalization of 6H-SiC using organophosphonate monolayers. *Appl. Phys. Lett.* **2012**, *100*, 101601.

(19) van den Berg, S. A.; Alonso, J. M.; Wadhwa, K.; Franssen, M. C. R.; Wennekes, T.; Zuilhof, H. Microwave-Assisted Formation of Organic Monolayers from 1-Alkenes on Silicon Carbide. *Langmuir* **2014**, *30*, 10562−10565.

(20) Howgate, J.; Schoell, S. J.; Hoeb, M.; Steins, W.; Baur, B.; Hertrich, S.; Nickel, B.; Sharp, I. D.; Stutzmann, M.; Eickhoff, M. Photocatalytic Cleavage of Self-Assembled Organic Monolayers by UV-Induced Charge Transfer from GaN Substrates. *Adv. Mater.* **2010**, *22*, 2632−2636.

(21) Morisaki, H.; Ono, H.; Yazawa, K. Photoelectrochemical Properties of Single-Crystalline n-SiC in Aqueous Electrolytes. *J. Electrochem. Soc.* **1984**, *131*, 2081−2086.

(22) van de Lagemaat, J.; Vanmaekelbergh, D.; Kelly, J. J. Photoelectrochemical characterization of 6H−SiC. *J. Appl. Phys.* **1998**, *83*, 6089−6095.

(23) Schnabel, C.; Wörner, M.; González, B.; del Olmo, I.; Braun, A. M. Photoelectrochemical characterization of p- and n-doped single crystalline silicon carbide and photoinduced reductive dehalogenation of organic pollutants at p-doped silicon carbide. *Electrochim. Acta* **2001**, *47*, 719−727.

(24) van Dorp, D. H.; Kelly, J. J. Photoelectrochemistry of 4H−SiC in KOH solutions. *J. Electroanal. Chem.* **2007**, *599*, 260−266.

(25) Chen, S.; Wang, L.-W. Thermodynamic Oxidation and Reduction Potentials of Photocatalytic Semiconductors in Aqueous Solution. *Chem. Mater.* **2012**, *24*, 3659−3666.

(26) Shor, J. S.; Grimberg, I.; Weiss, B.-Z.; Kurtz, A. D. Direct observation of porous SiC formed by anodization in HF. *Appl. Phys. Lett.* **1993**, *62*, 2836−2838.

(27) Shor, J. S.; Kurtz, A. D. Photoelectrochemical Etching of 6H-SiC. *J. Electrochem. Soc.* **1994**, *141*, 778−781.

(28) Shor, J. S.; Zhang, X. G.; Osgood, R. M. Laser-Assisted Photoelectrochemical Etching of n-type Beta-SiC. *J. Electrochem. Soc.* **1992**, *139*, 1213−1216.

(29) Shishkin, Y.; Choyke, W. J.; Devaty, R. P. Photoelectrochemical etching of n-type 4H silicon carbide. *J. Appl. Phys.* **2004**, *96*, 2311−2322.

(30) McDonald, K. J.; Choi, K.-S. Photodeposition of Co-Based Oxygen Evolution Catalysts on α-Fe_2O_3 Photoanodes. *Chem. Mater.* **2011**, *23*, 1686−1693.

(31) Kanan, M. W.; Nocera, D. G. In Situ Formation of an Oxygen-Evolving Catalyst in Neutral Water Containing Phosphate and Co2+. *Science* **2008**, *321*, 1072−1075.

(32) Reece, S. Y.; Hamel, J. A.; Sung, K.; Jarvi, T. D.; Esswein, A. J.; Pijpers, J. J. H.; Nocera, D. G. Wireless Solar Water Splitting Using Silicon-Based Semiconductors and Earth-Abundant Catalysts. *Science* **2011**, *334*, 645−648.

(33) Horcas, I.; Fernández, R.; Gómez-Rodríguez, J. M.; Colchero, J.; Gómez-Herrero, J.; Baro, A. M. WSXM: A software for scanning probe microscopy and a tool for nanotechnology. *Rev. Sci. Instrum.* **2007**, *78*, 013705.

(34) Nozik, A. J.; Memming, R. Physical Chemistry of Semiconductor−Liquid Interfaces. *J. Phys. Chem.* **1996**, *100*, 13061−13078.

(35) Memming, R. *Semiconductor Electrochemistry*; Wiley-VCH Verlag GmbH: Weinheim, Germany, 2000.

(36) Morrison, S. R. *The Chemical Physics of Surfaces*; Springer: Boston, MA, 1977.

(37) Winnerl, A.; Pereira, R. N.; Stutzmann, M. Kinetics of optically excited charge carriers at the GaN surface. *Phys. Rev. B: Condens. Matter Mater. Phys.* **2015**, *91*, 075316.

(38) Gärtner, W. W. Depletion-Layer Photoeffects in Semiconductors. *Phys. Rev.* **1959**, *116*, 84−87.

(39) Choyke, W.; Patrick, L. Higher Absorption Edges in 6H SiC. *Phys. Rev.* **1968**, *172*, 769−772.

(40) Schäfer, S.; Koch, A. H. R.; Cavallini, A.; Stutzmann, M.; Sharp, I. D. Charge Transfer across the n-Type GaN−Electrolyte Interface. *J. Phys. Chem. C* **2012**, *116*, 22281−22286.

(41) The atomic scale terraces visible on the micrograph originate from a slight wafer offcut from the (0001) direction, resulting in bilayer transitions at the SiC surface.

(42) Pijpers, J. J. H.; Winkler, M. T.; Surendranath, Y.; Buonassisi, T.; Nocera, D. G. Light-induced water oxidation at silicon electrodes functionalized with a cobalt oxygen-evolving catalyst. *Proc. Natl. Acad. Sci. U. S. A.* **2011**, *108*, 10056−10061.

(43) Zhong, D. K.; Sun, J.; Inumaru, H.; Gamelin, D. R. Solar Water Oxidation by Composite Catalyst/α-Fe_2O_3 Photoanodes. *J. Am. Chem. Soc.* **2009**, *131*, 6086−6087.

(44) Steinmiller, E. M. P.; Choi, K.-S. Photochemical deposition of cobalt-based oxygen evolving catalyst on a semiconductor photoanode

DOI: 10.1021/acs.langmuir.5b04376
Langmuir 2016, 32, 1637−1644

for solar oxygen production. *Proc. Natl. Acad. Sci. U. S. A.* **2009**, *106*, 20633−20636.
(45) Hornetz, B.; Michel, H.-J.; Halbritter, J. Oxidation and 6H-SiC−SiO_2 interfaces. *J. Vac. Sci. Technol., A* **1995**, *13*, 767−771.
(46) We note that, for the Co−Pi-functionalized SiC electrode, the O1s peak can also be affected by oxygen atoms from the catalyst. However, because the corresponding binding energy is expected to be very similar to the O1s signal originating from the hydroxyl surface termination of the SiC electrodes and from adsorbed water molecules, the contribution of the Co−Pi catalyst to the overall O1s signal cannot be resolved as a separate component in Figure 6.

DOI: 10.1021/acs.langmuir.5b04376
Langmuir 2016, 32, 1637−1644